Synergistically improving open-circuit voltage and fill factor via utilizing a natural pigment as efficient interconnect layer for high-performance

Chemical Engineering Journal 522 (2025) 167241

Contents lists available at ScienceDirect

Chemical Engineering Journal

journal homepage: www.elsevier.com/locate/cej

Synergistically improving open-circuit voltage and fill factor via utilizing a natural pigment as efficient interconnect layer for high-performance perovskite-organic tandem solar cells

Bin Zhang [a,*], Yunqiang Du [a], Xinling Li [a], Aiqin Li [a], Menglan Lv [a,*], Weile Guo [a], Fei Guo [c,*], Ergang Wang [b,*]

[a] Engineering Research Center for Energy Conversion and Storage Technology of Guizhou, School of Chemistry and Chemical Engineering, Guizhou University, Guiyang 550025, China
[b] Department of Chemistry and Chemical Engineering, Chalmers University of Technology, SE-412 96 Göteborg, Sweden
[c] Institute of New Energy Technology, College of Information Science and Technology, Jinan University, Guangzhou 510632, China

ARTICLE INFO

Keywords:
Cathode interfacial layer
High open-circuit voltage
Interconnect layer
Laccaic acid
Perovskite-organic tandem solar cells

ABSTRACT

Cathode interfacial layer (CIL) plays an indispensable role in improving power conversion efficiency (PCE) for perovskite solar cells (PSCs). To acquire low-cost, environmentally friendly and effective cathode interfacial materials (CIMs), a natural pigment, laccaic acid (LA), is utilized as CIL for achieving high-performance PSCs. Attributing to the introduction of LA CIL, the work function (*WF*) of silver cathode is decreased obviously, leading to better interfacial ohmic contact. This lower *WF* in cathode could facilitate electron transport, resulting in distinct suppression in charge recombination and energy loss. As a result, the introduction of LA CIL improves the photovoltaic performance effectively in 1.77 eV wide bandgap PSCs with a high open-circuit voltage (V_{OC}) of 1.32 V, a high fill factor (FF) of 81 % and a PCE of 18.48 %. Interestingly, LA shows a broad application as interconnect layer (ICL) in perovskite-organic tandem solar cells (POTSCs), in which it results in a high PCE of 23.51 % with a V_{OC} of 2.15 V. This V_{OC} is one of the highest values in POTSCs. Hence, LA exhibits a promising feature as a natural product to construct CIL and ICL in solar cells for realizing a low-cost, green and sustainable photovoltaic technology.

1. Introduction

Solar cells, as one of the efficient technologies for converting solar energy into electricity, are developed rapidly during last decades. Among these solar cells, perovskite solar cells (PSCs) as an emerging technology have attracted much attention both academically and commercially, ascribing to their advantages in feasibly accessible resources, low cost, solution process and large-scale fabrication [1,2]. Till now, the power conversion efficiencies (PCEs) of conversional and inverted PSCs (i-PSCs) have exceeded 26 %, which positions it as a competitive candidate for commercial application [3–5].

Recently, the i-PSCs [6,7], typically containing the device architecture of ITO/hole transport layer (HTL)/perovskite layer/electron transport layer (ETL)/cathode interfacial layer (CIL)/cathode, have been investigated intensively due to their merits in feasible fabrication, high stability and excellent compatibility in tandem solar cells (TSCs) [8] including perovskite-perovskite TSCs (PPTSCs) [9,10], perovskite-organic TSCs (POTSCs) [11,12] and perovskite-silicon TSCs (PSTSCs) [13–16]. Comparing to the PPTSCs and PSTSCs, the POTSCs offer advantages of lower production costs, flexibility, lightweight design, and greater material tunability, making them a more cost-effective and versatile alternative, particularly for flexible and environmentally friendly applications [17]. Furthermore, POTSCs combine the strengths of both perovskite and organic technologies, where wide-bandgap PSCs serve as a front cell for absorbing short-wavelength light, while versatile low-bandgap OSCs function as a rare cell for absorbing longer wavelengths. This complementary absorption enables full-spectrum solar coverage and, therefore, high photovoltaic performance can be expected from POTSCs [18,19].

It is noted that the interfacial layers in the PSCs play a crucial role in achieving high photovoltaic performance, which could tune the electrode work function (*WF*), passivate interfacial defects, protect active

* Corresponding authors.
E-mail addresses: zhangb@gzu.edu.cn (B. Zhang), mllv@gzu.edu.cn (M. Lv), feiguo@jnu.edu.cn (F. Guo), ergang@chalmers.se (E. Wang).

https://doi.org/10.1016/j.cej.2025.167241
Received 22 December 2024; Received in revised form 3 June 2025; Accepted 13 August 2025
Available online 14 August 2025

layer and so on. As a result, a good interface would elevate the photovoltaic performance remarkably by reducing charge recombination, but a poor interface may interfere charge extraction and attenuate device performance dramatically [20–22]. Therefore, the interface engineering is an indispensable process for attaining high photovoltaic performance in PSCs. Among these interfaces, the cathode interface is one of very prominent interfaces in PSCs, which have been studied widely in the recent years [23]. To find useful cathode interfacial materials (CIMs), many inorganics, small molecules and polymers have been developed successfully. Preliminarily, the *n*-type semiconducting metal oxides are one kind of potential CIMs which can be used in PSCs, such as ZnO [24], TiO*x* [22] and MXene [25,26]. Moreover, semiconducting organics and polymers are also developed widely to work as CILs in PSCs because of their merits in feasibly chemical functionalization, solution processibility and easy energy level tunability, such as fullerene derivatives [27], perylene diimide derivatives [28–30] and naphthalene diimide-based polymers [31]. Among these organic and polymeric CIMs, the most widely used are phenanthroline-based small molecules, such as 2,9-dimethyl-4,7-diphenyl-1,10-phenanthroline (BCP) [32] and 4,7-diphenyl-1,10-phenanthroline (Bphen) [33] and 4,7-dimethoxy-[1,10] phenanthroline (Phen-OMe) [34], attributing to their suitable energy levels and operatable synthesis. Even though these small molecules and polymers could realize high efficiency in PSCs, they also suffer from an inevitable disadvantage of which these CIMs should be chemically synthesized via complicated routes, leading to high cost and large environmental footprint. Therefore, it is urgent to develop a new methodology to fabricate environmentally friendly CIMs in PSCs.

Interestingly, some natural products (NPs) are promising material resources that are inherently green and biocompatible, and they have been widely utilized, particularly in the food industry. It is widely known that there exist many kinds of polar groups in NPs, such as hydroxyl, carboxyl, amino and carbonyl, which would potentially interact with perovskite layer or metal electrodes to improve photovoltaic performance. For instance, the introduction of NPs, such as caffeine [35], natural piperine [36] and vitamin [37], can passivate the interfacial defects of perovskite layer; and the NPs also worked as an interfacial passivator for buried interface, such as cobalamin [38] and citric acid [39].

These diverse achievements in interfacial passivation using NPs highlight their potential as excellent interfacial materials for PSCs. In this study, we introduce a natural pigment, laccaic acid (LA), extracted from the natural shellac, as CIL in PSCs (as presented in Fig. 1 and

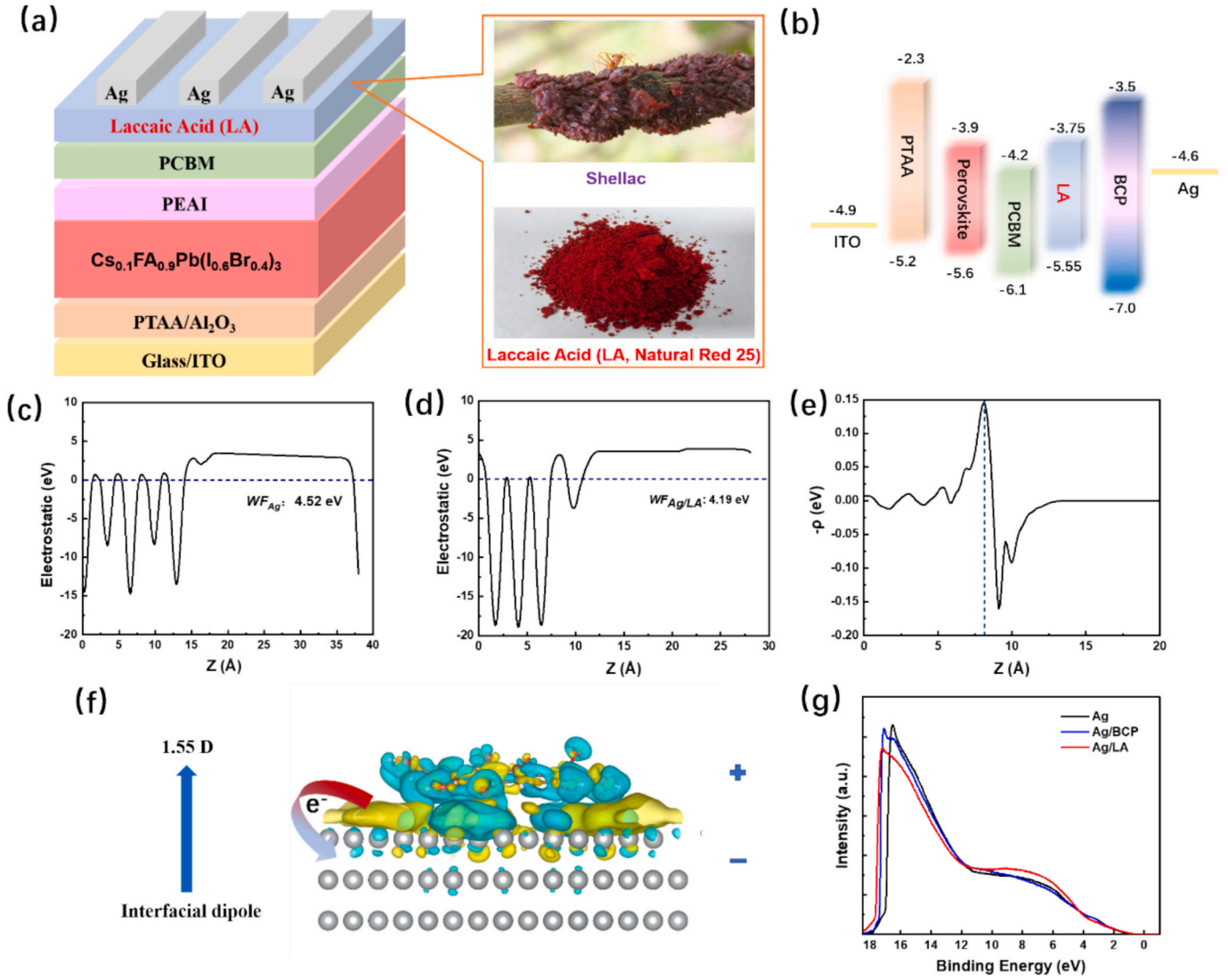

Fig. 1. (a) The device structure of i-PSCs and the photographs of shellac and LA; (b) energy level diagram; the work functions of theoretical calculation for (c) neat Ag, (d) LA modified Ag; (e) charge density redistribution on the surface of Ag (111) with LA modification; (f) proposed work mechanism of the interfacial dipoles of LA on the surface of Ag (111); and (g) the UPS curves of neat Ag, and BCP and LA modified Ag.

Fig. S2). Characterization reveals that LA contains several polar groups, including hydroxyl, carboxyl, and carbonyl groups, which can effectively interact with the silver (Ag) cathode. Through introducing LA as CIL between ETL and Ag cathode, a distinctly interfacial dipole is formed, resulting in the obvious decrease in *WF* of Ag. Owing to the lowered *WF* of Ag, it facilitates the electron transport at interface and forms better ohmic contact between ETL and cathode, leading to the lower interfacial energy loss, and ultimately realizing higher PCE in wide-bandgap (WBG) PSCs. When a perovskite layer with a wide band gap of 1.77 eV is utilized as active layer in i-PSCs, the PCE is improved to 18.48 % with a high open-circuit voltage (V_{OC}) of 1.32 V and a high fill factor (FF) of 81 % as compared to the control device without LA (a PCE of 15.39 %, a V_{OC} of 1.26 V and an FF of 73 %). Interestingly, the introduction of LA as CIL enhances both V_{OC} and FF simultaneously in the resulting devices. To the best of our knowledge, this V_{OC} is one of the highest values for WBG PSCs (refer to Table S3). Furthermore, LA displays broader applicability as interfacial layers, where it could work as efficient interconnect layer (ICL) in POTSCs. Through introducing LA into the ICL, the POTSCs show a high PCE of 23.51 % with V_{OC} of 2.15 V and short-circuit current density (J_{SC}) of 14.91 mA cm^{-2}. Hence, these results demonstrate that the natural pigment LA can work as efficient CILs in PSCs and ICLs in POTSCs, which position it as a competitive candidate for functional layers instead of the chemically synthesized materials for achieving high-performance PSCs.

2. Results and discussion

2.1. Theoretical calculation and work mechanism

To investigate the photovoltaic performance of LA as CIL, the i-PSCs with the device structure of ITO/PTAA/Al_2O_3/$Cs_{0.1}FA_{0.9}Pb(I_{0.6}Br_{0.4})_3$/PEAI/PCBM/LA/Ag was constructed, where the $Cs_{0.1}FA_{0.9}Pb(I_{0.6}Br_{0.4})_3$ worked as a WBG perovskite layer and PEAI as a passivating layer, as presented in Fig. 1a. Here, LA is a natural pigment which is from the natural shellac. It is widely known that LA is denoted as natural red 25, which is used widely in food and medical industries as a green additive. Comparing to the widely used CILs such as BCP and Bphen, LA shows a low-cost advantage (as presented in Table S1). Therefore, LA is an environmentally friendly organic material for developing sustainable photovoltaic technology. To get the highest occupied molecular orbital (HOMO) and lowest unoccupied molecular orbital (LUMO) energy levels of LA, the electrochemical measurement was carried out, as shown in Fig. S1. It is found that the HOMO and LUMO energy levels of LA are located at −5.55 and − 3.75 eV, respectively, and the related energy level diagram are presented in Fig. 1b.

It is noted that the existence of CIL in PSCs would affect the *WF*s of the Ag cathode, which would play a key role in the determination of the performance of PSCs [40]. To investigate influence of LA on Ag cathode, both theoretical calculation (the simplified chemical structure was presented in Fig. S2) and ultra-violet photoelectron spectrometer (UPS) test were conducted to evaluate the *WF*s, as shown in Fig. 1(c-g). The calculated *WF* of pristine Ag (111) is 4.52 eV, which agrees well with the result reported in literature [41,42], while the introduction of LA as a modifier on the Ag interface leads to a down shift of *WF* to 4.19 eV, which is 0.33 eV lower than that of pristine Ag cathode. This reduction of *WF* is possibly owing to the formation of interfacial dipole at the Ag interface. To verify this dipole formation, an electron density distribution was theoretically calculated, as presented in Fig. 1e. It is shown that a distinct electron transfer process from the LA layer to Ag cathode occurs, resulting in an apparent electron density variation near the Ag (111) interface (~8 Å). This result implies that the electron transfer would happen in about 8 Å length, and thus the interfacial dipole is formed among this length scale. To further elucidate this electron density distribution for forming interfacial dipole, the interfacial dipole Δμ at the Ag (111) interface with LA was calculated, as displayed in Fig. 1f. It is noted that a Δμ of 1.55 D is formed with the distinct upward direction from Ag to LA, which is the direct nature of the interfacial dipole, leading to the obvious *WF* reduction of LA-modified Ag cathode. To verify the results from theoretical calculation, the UPS test was carried out, as displayed in Fig. 1(g). It is featured that the binding energies of BCP and LA modified Ag surfaces are shifted to the higher values, leading to the distinct *WF*s reduction of Ag to 4.18 and 4.11 eV for BCP and LA, respectively, whereas the bare Ag shows a higher *WF* of 4.62 eV. To further verify the *WF* difference caused by the introduction of LA, the Kelvin probe force microscope (KPFM) test was used to measure the *WF*s of Ag, where the bare Ag gives a *WF* of 4.56 eV and a LA-modified Ag shows a lower *WF* of 4.36 eV. Clearly, the introduction of CILs, especially for LA, would lower the *WF* of Ag cathode effectively, resulting from the formation of right interfacial dipoles at the Ag interface. Subsequently, these suitable low *WF*s would improve the interfacial ohmic contact between active layer and cathode, facilitating efficient electron extraction and transport, thereby realizing high V_{OC}, FF and PCE in PSCs.

2.2. Photovoltaic performance

To evaluate the CIL characteristics, the photovoltaic performance was measured, and the *J-V* curves were presented in Fig. 2a, and the corresponding statistical data were shown in Fig. S3 and S4. To optimize the fabrication condition, the effect of different LA concentrations on photovoltaic performance was also investigated, as shown in Fig. S5, and the corresponding data were summarized in Table S2. It is found that the LA concentration with 0.5 mg ml^{-1} presents the best photovoltaic performance. As a comparison, the widely used CIL of BCP was also utilized here as a control device. It is shown that the photovoltaic performance is improved dramatically when the CILs of BCP or LA are introduced in i-PSCs, where the PCEs are increased to 18.27 % and 18.48 % for BCP and LA, respectively. While the device without any CIL only gives a low PCE of 15.39 %. Interestingly, the device with LA as CIL exhibits the highest photovoltaic performance with impressively high V_{OC} of 1.32 V and FF of 81 % as compared to the devices without and with BCP as CIL. Moreover, the PSCs incorporating LA as the CIL exhibit high performance reproducibility, as shown in Fig. S4, highlighting the strong potential of LA as an excellent CIL. Furthermore, LA-based PSC shows the lowest hysteresis effect, as presented in Fig. S6 and Table 1. In Fig. 2b, it displays the external quantum efficiency (EQE) curves of i-PSCs, illustrating that the PSCs show a wide-range light response from 300 to 700 nm. Importantly, the devices with BCP and LA present the highest light-to-electric conversion efficiencies, exceeding 80 %. Especially, the EQEs reach about 90 % at around 400–550 nm. These high EQE response would result in high J_{SC}, and the integrated J_{SC}s from EQE curves are consistent with the results from *J-V* curves. In Fig. 2c, it showed the stabilized power output (SPO) curves for the PSCs without CILs, and with BCP or LA as CILs, respectively. In addition, the device shelf lifetime test was carried out, as present in Fig. S7. It shows that the introduction of CILs would improve the device shelf lifetime obviously, where the LA-modified device gives the highest lifetime than control and BCP-modified devices, indicating that LA is an excellent interfacial layer for improving photovoltaic performance. Apparently, the device with LA as CIL presents the highest device shelf lifetime than those of devices without CIL, and with BCP as CIL, depicting that the LA could realize stable photovoltaic performance in i-PSCs [43,44]. To evaluate the results in this work, the comparison of band gap-V_{OC}-PCE statistics in wide bandgap based i-PSCs was summarized, as displayed in Fig. 2d and Table S3. To the best of our knowledge, this photovoltaic performance is one of the best values for WBG i-PSCs.

2.3. Surface morphology investigation

It is widely known that the surface morphology of active layer plays a significant role in achieving high-performance PSCs, whereas optimal surface morphology would promote photovoltaic characteristics

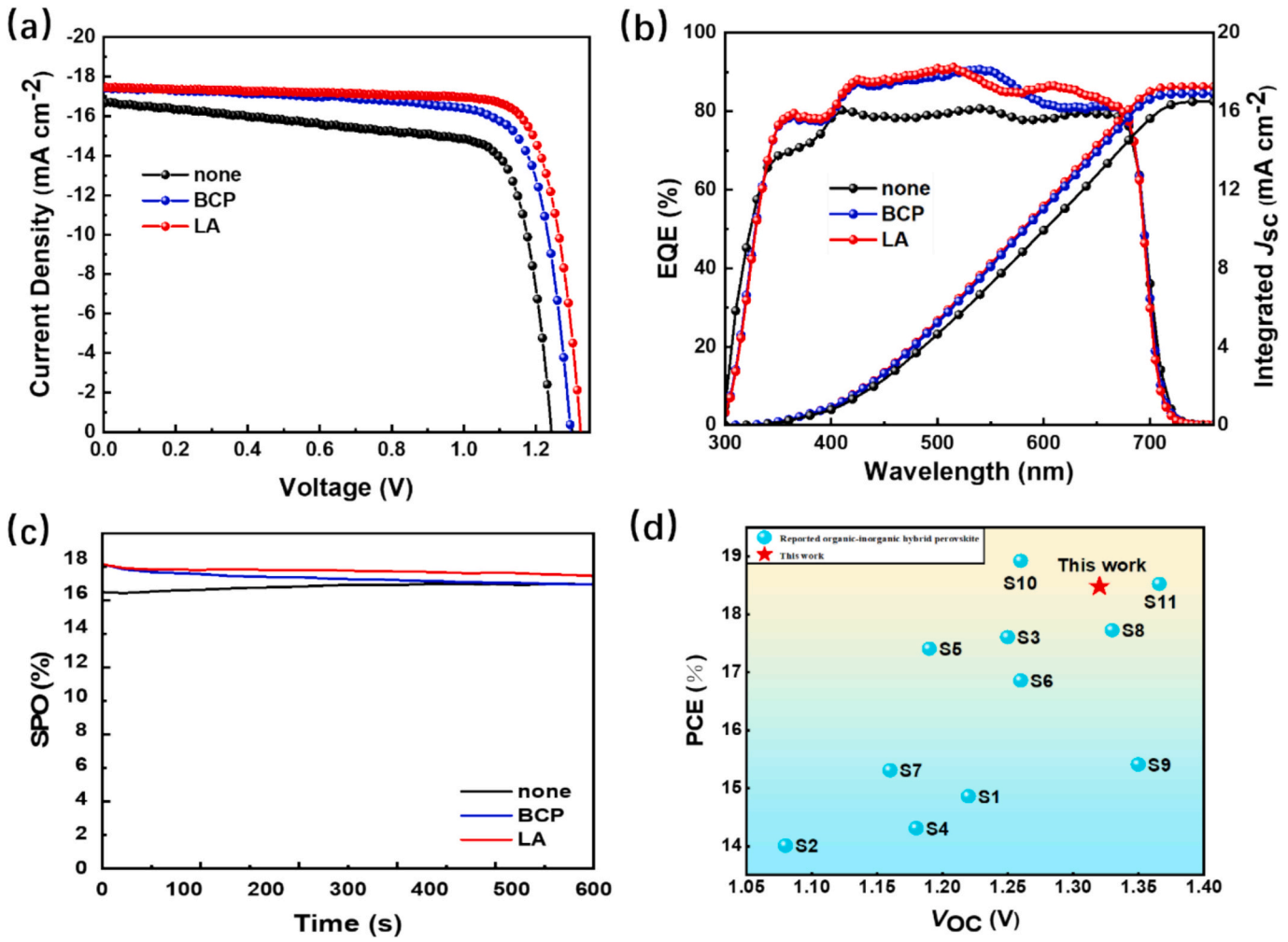

Fig. 2. (a) *J-V*, (b) EQE and (c) SPO curves for the PSCs without and with BCP and LA as CILs, respectively; (d) The literature comparison of band gap-V_{OC}-PCE statistics in wide bandgap (1.6–1.9 eV) based i-PSCs, and the red star represents the photovoltaic performance in this work.

Table 1
Summary of photovoltaic properties based on the devices with different CILs under AM 1.5 G, 100 mw cm^{-2}.

CILs	Scan direction	V_{oc} (V)	J_{sc} (mA cm^{-2})	J^{b}_{sc} (mA cm^{-2})	FF (%)	PCE$^{a}_{avg}$ (%)	PCE$_{max}$ (%)
none	FS	1.26	16.56	16.49	69	15.07 (±0.3)	14.70
	RS	1.26	16.51		73	15.11 (±0.4)	15.39
BCP	FS	1.31	17.55	17.24	77	17.85 (±0.1)	17.93
	RS	1.30	17.57		80	18.07 (±0.2)	18.27
LA	FS	1.32	17.54	17.23	80	18.19 (±0.2)	18.42
	RS	1.32	17.50		81	18.23 (±0.2)	18.48

The FS and RS represent the forward scan and reverse scan, respectively.
a) The average PCE values from 10 individual devices.
b) Integrated J_{SC} from EQE curves.

tremendously. Therefore, atomic force microscopy (AFM) and scanning electron microscopy (SEM) were carried out to investigate the surface morphology under the device structure of ITO/PTAA/Al_2O_3/perovskite/PCBM/CILs, as presented in Fig. 3. The AFM images indicate that the pristine film without CIL presents a rough surface with root-mean-square (rms) roughness of 9.11 nm, while the rms roughness of the devices with BCP and LA as CILs decrease to 6.24 and 5.81 nm, respectively. Interestingly, the LA modified surface displays the lowest rms roughness, which would be beneficial for forming optimal interface between PCBM and Ag cathode, and thereby promoting interfacial electron transport and minimizing interfacial energy loss. Surprisingly, the surfaces of PCBM layers with BCP and LA as modifiers visualize large-scale domains and much more continuous feature, specifically for LA-modified surface, indicating that this excellent surface is preferable to electron transport and impeding interfacial energy loss. Moreover, the X-ray photoelectron spectroscopy (XPS) measurement was also utilized to verify the interaction between LA and Ag, as shown in Fig. S8 [45]. It illustrates that the binding energy of Ag 3d of pristine Ag without LA modification is 368.0 eV, but the binding energy of Ag 3d is shifted to 367.7 eV when the Ag electrode is modified by LA. This result implies that the LA can interact with Ag effectively. To further investigate the coverage of CIL layers, the test of water contact angles was performed, as presented in Fig. 3(d-f). The water contact angle of pristine PCBM layer is 100.6°, while those of CILs-modified PCBM layers with BCP and LA are decreased to 95.7° and 80.9°, respectively, which implies that the CILs can deposit on the PCBM layer efficiently. Hence, the LA as CIL could improve PCBM surface, which is potentially beneficial for achieving high photovoltaic performance in i-PSCs.

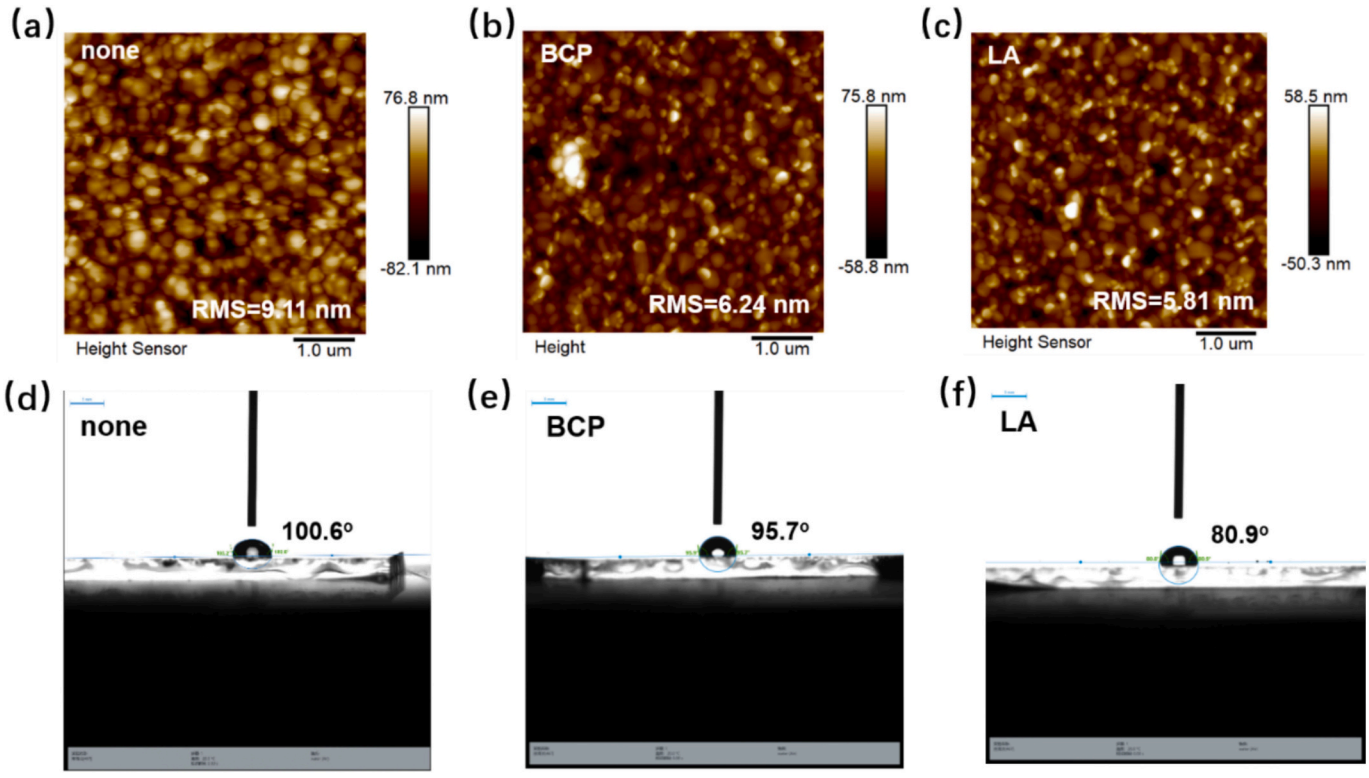

Fig. 3. (a-c) AFM (size: 5 μm × 5 μm) and (d-f) water contact angles for the surfaces without CIL and with BCP and LA as CILs, respectively, under the device structure of ITO/PTAA/Al_2O_3/perovskite/PCBM/CILs.

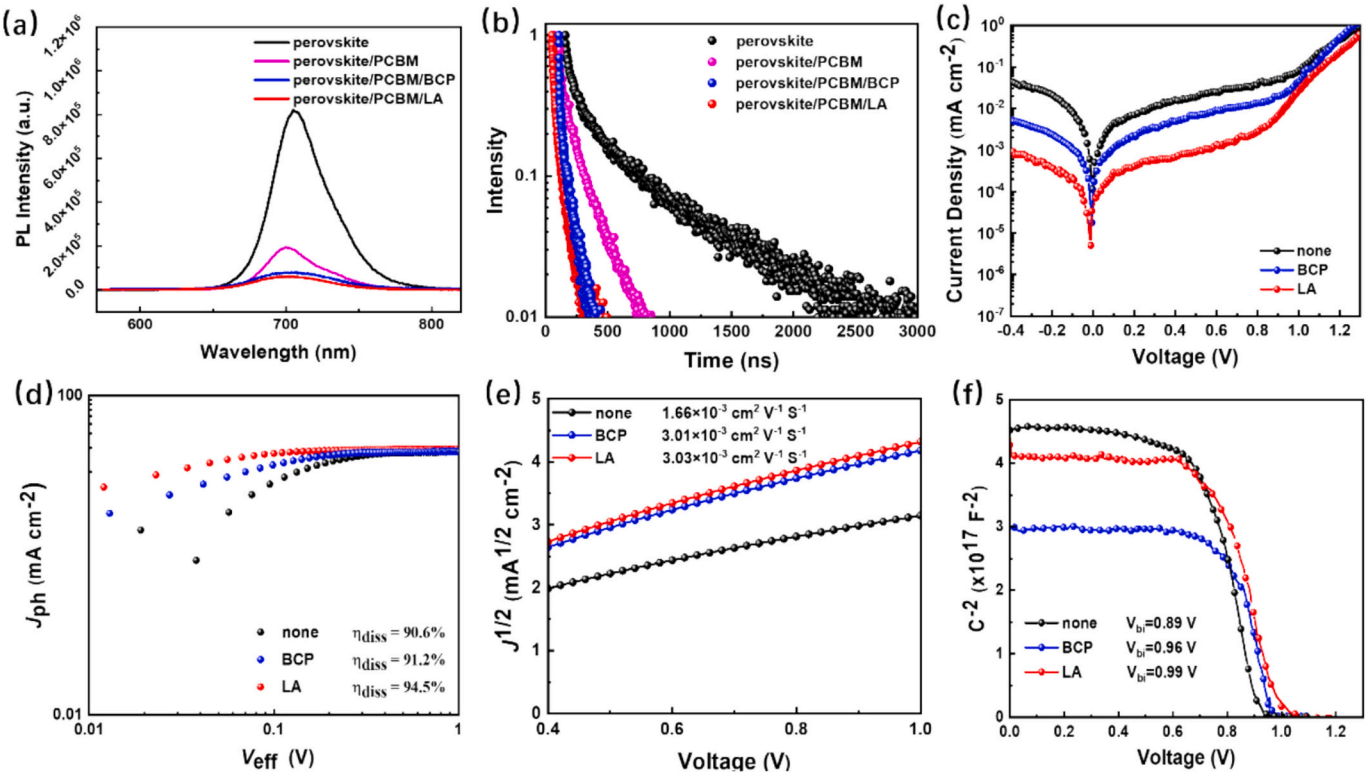

Fig. 4. (a) PL and (b)TRPL spectra, (c) *J-V* curves in the dark, (d) J_{ph}-V_{eff} curves, (e) $J^{1/2}$-*V* curves from electron-only device for PCBM, and (f) Mott-Schottky characteristics for the PSCs without and with BCP and LA as CILs, respectively.

2.4. Charge carrier dynamics

As mentioned above, the introduction of LA CIL has improved the photovoltaic performance in i-PSCS. To understand the nature of LA function, the investigation on charge carrier dynamics were carried out, as presented in Figs. (4 and 5). In Fig. 4(a), it gives the photoluminescence (PL) spectra of the perovskite films with PCBM and CILs. It is noted that the pristine perovskite layer shows a high PL emission, whereas the PL is quenched dramatically when PCBM is added; moreover, the PL is quenched further when CILs of BCP and LA are covered atop the PCBM layer, indicating that the CILs could enhance the electron transfer and transport at interface efficiently. This effect can be reflected from the time-resolved photoluminescence (TRPL) spectra obviously, as shown in Fig. 2(b). It is clear that the lifetime of pristine perovskite is about 150 ns, but when the PCBM layer is covered on perovskite, the lifetime is decreased to 119 ns, implying the efficient charge transfer occurred. Notably, the lifetimes are further decreased to 48 and 22 ns for the composite films with BCP and LA as CILs, respectively, indicating that the CILs would facilitate interfacial electron transport, which is consisted with the results from photovoltaic devices [46]. To understand the charge carrier transport in the device, the *J-V* curves in dark were measured, as displayed in Fig. 2(c). Comparing to the PSC device without CIL, it is observed that the devices with CILs modification exhibit largely reduced reverse saturation current densities (RSCDs). Specifically, the device with LA as CIL shows the lowest RSCD, ascribing to the improved interfacial ohmic contact and decreased *WF* of Ag cathodes [47]. To further clarify the effects of different CILs on PSCs, the tests of photogenerated current density (J_{ph}) vs effective voltage (V_{eff}) were carried out, as presented in Fig. 2(d). This effect would account for the related charge dissociation and collection efficiency. It is noted that the photogenerated current densities among these three kinds of devices without CIL and with BCP and LA as CILs could reach the corresponding saturation (J_{sat}) at high V_{eff}, suggesting that the exciton dissociation and collection are efficient enough. Through the calculation, the exciton dissociation rates (η_{diss}) are 90.6 %, 91.2 % and 94.5 % for bare Ag, and with BCP and LA as CILs, respectively. It illustrates that the LA modified device gives the highest η_{diss}, indicating that the new LA-based CIL could promote the exciton dissociation ability efficiently in PSCs. It is known that the introduction of CIL in PSCs could improve the electron mobility (μ_e) of PCBM. Here, the space-charge limited current (SCLC) method was applied to record the μ_es of PCBM, where the electron-only devices were constructed under the device architecture of ITO/SnO_2/PCBM/CIL/Ag, as shown in Fig. 4(e). It is noted that the pristine PCBM without any CIL modification gives the μ_e of 1.66 × 10^{-4} cm^2 V^{-1} s^{-1}, but the μ_es of PCBM layers with modification of BCP and LA are increased to 3.01 × 10^{-4} and 3.03 × 10^{-4} cm^2 V^{-1} s^{-1}, respectively, indicating that the introduction of CILs would enhance the μ_e of PCBM layer efficiently which is beneficial for facilitating electron transport and inhibiting interfacial recombination. To investigate the carrier separation and transport, the Mott-Schottky curves was performed for extracting the built-in potentials (V_{bi}s) in the devices, as displayed in Fig. 4(f). It shows that the V_{bi}s for the devices without CIL, and with BCP and LA as CILs, are 0.89, 0.96 and 0.99 V, respectively. It is obvious that the V_{bi} of LA-modified device is superior to the other two devices, implying that this device poses the highest internal driving force for carrier separation and transport [48]. Hence, this highest V_{bi} in LA-based device leads to the highest V_{OC} in PSCs, which is consistent to the results extracted from *J-V* curves in Fig. 2(a).

To investigate the charge carrier recombination in the devices, the V_{OC}s and J_{SC}s variation under different light intensity were performed, as presented in Fig. 5(a&b). In Fig. 5(a), it gives the V_{OC}s-light intensity relationship, where it follows the formula of $V_{OC} \propto nkTln(I)/q$. It is noted that the slop constants are 1.34kT/q, 1.28kT/q and 1.13kT/q for the devices without CIL, and with BCP and LA as CILs, respectively. Obviously, the LA-modified device shows the lowest slop, implying that the introduction of LA as CIL could impede the trap-assisted recombination in the PSCs [49]. Additionally, to further study the internal bimolecular recombination in the PSCs, the J_{SC}-light intensity relationship was

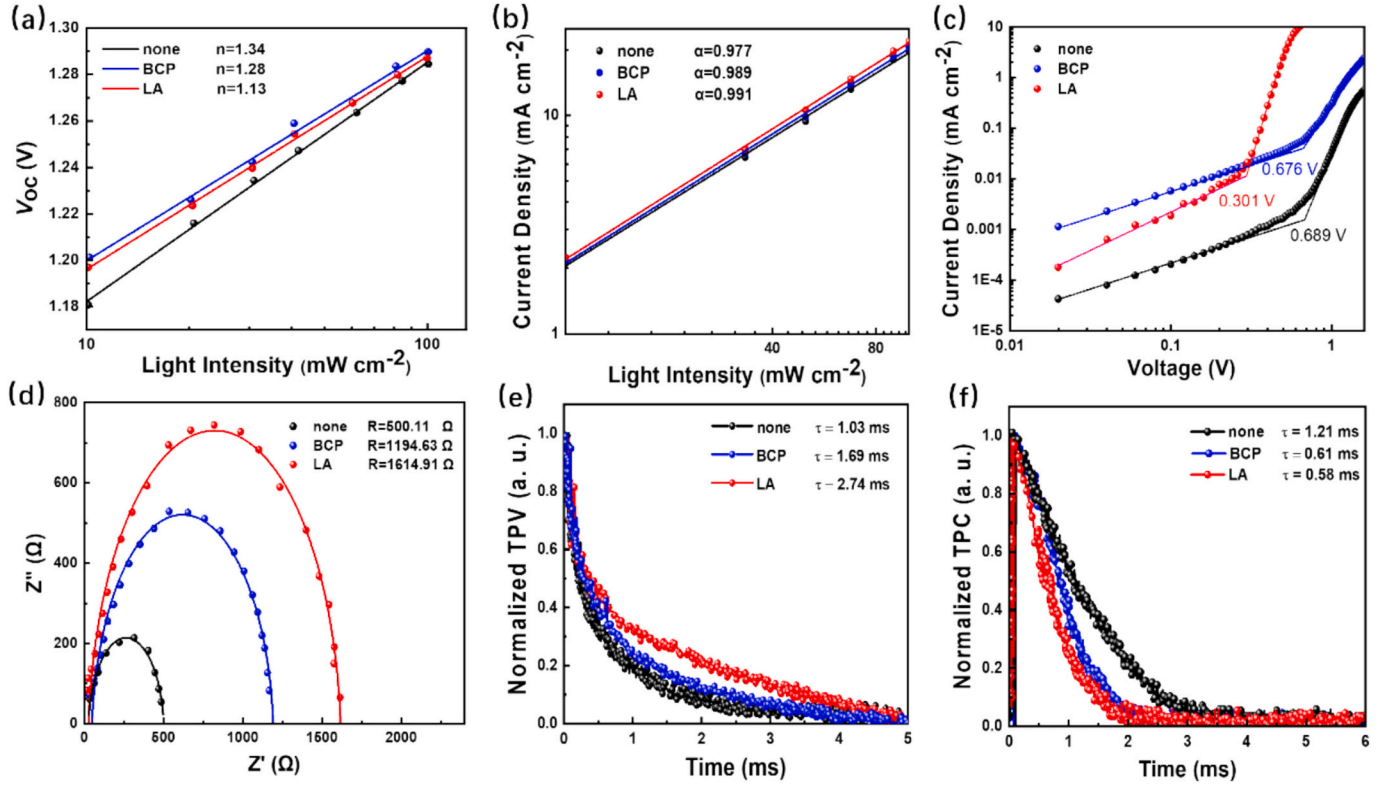

Fig. 5. (a) V_{OC}-light intensity (ln I) and (b) J_{SC}-light intensity characteristics, (c) *J-V* curves in dark of the electron-only device for perovskite layer, (d) Nyquist plots in dark and charge carrier dynamics test for (e) TPV-time and (f) TPC-time characteristics.

tested, where it follows the power law of $J_{SC} \propto I^{\alpha}$, as shown in Fig. 5(b). It is well-known that if the slope in J_{SC}-light intensity relationship is approaching to 1, it manifests that the bimolecular recombination would be absent in the device. As presented in Fig. 2(b), the slopes for bare Ag, BCP and LA modified devices are 0.977, 0.989 and 0.991, respectively, suggesting LA-based CIL can suppress the bimolecular recombination more effectively, and ultimately obtain the highest photovoltaic performance. To quantitatively investigate the trap-state density in PSCs, the electron-only devices under the architecture of ITO/SnO_2/perovskite/CIL/Ag were adopted, as presented in Fig. 5(c). The trap-filled limited voltages (V_{TFL}s) for the devices without CIL and with BCP and LA as CILs are 0.689, 0.676 and 0.301 V, corresponding to the related trap densities (n_ts) of 2.96 × 10,[16] 2.91 × 10^{16} and 1.29 × 10^{16} cm^{-3}, respectively. It shows that the device with LA as CIL exhibits the lowest n_t than the other two devices, suggesting that LA-modified device could passivate the traps efficiently and thus suppress the interfacial recombination [50]. Moreover, the electrochemical impedance spectroscopy (EIS) test was also carried out to study the electron transport and recombination dynamics in PSCs, and the related Nyquist plots were presented in Fig. 5(d). It illustrates that the recombination resistances (R_{rec}s) for the control device, and BCP and LA modified devices are 500.11, 1194.63 and 1614.91 Ω, respectively. Evidently, the LA-based device shows the highest R_{rec} than control and BCP-modified devices, implying that the trap-assisted recombination is hindered at interface and the electron extraction and transport are promoted efficiently in PSCs [51]. To explore the charge extraction and recombination process comprehensively, the transient photovoltage (TPV) and transient photocurrent (TPC) were further carried out in detail, as shown in Fig. 5 (e&f). In Fig. 5(e), it gives the charge carrier decay lifetimes of the devices for control device and BCP and LA modified devices are 1.03, 1.69 and 2.74 ms, respectively. It is noted that the LA-based device has the highest decay lifetime, indicating enough time for charge carriers sweeping out from device, and inhibiting the interfacial recombination effectively. In addition, TPC was also utilized to evaluate the charge carrier extraction process of PSCs, as displayed in Fig. 5(f). It is observed that the charge carries extraction times with none, BCP and LA as CILs are 1.21, 0.61, and 0.58 ms, respectively, indicating that the LA-modified PSC extracts charge carriers out of device more efficiently. This fast charge carrier extraction would diminish the possibility of charge recombination, benefiting for the achievement on high

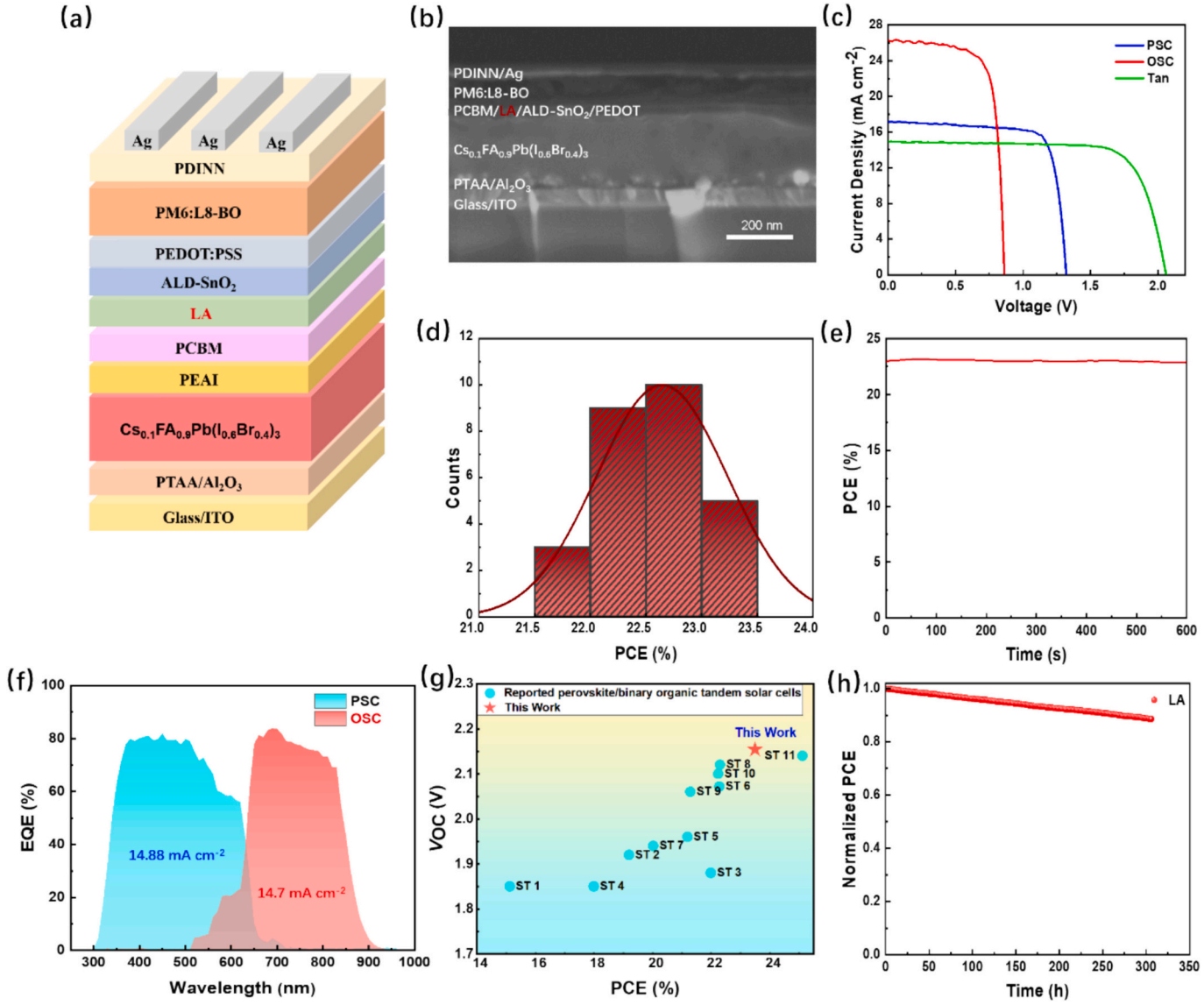

Fig. 6. (a) The device structure of POTSC, (b) the cross-section SEM image of POTSC, (c) *J-V* curves, (d) the statistic histogram of PCEs, (e) SPO curves, (f) EQE curves, (g) the literature comparison of V_{OC}-PCE statistics in the inverted perovskite-binary organic TSCs, and the red star represents the photovoltaic performance of POTSC in this work, and (h) the storage device shelf lifetime curves at 25 °C in nitrogen.

photovoltaic performance of LA-based PSC.

2.5. Investigation on perovskite-organic tandem solar cells

As mentioned above, the natural pigment LA can work as an efficient CIL in WBG PSCs via synergistic improvement on V_{OC} and FF. Therefore, it is potentially a novel candidate CIL to be utilized in ICL in POTSCs [52–54]. To explore the photovoltaic performance, the POTSC was fabricated within the device structure of ITO/PTAA/Al_2O_3/$Cs_{0.1}FA_{0.9}Pb(I_{0.6}Br_{0.4})_3$/PEAI/PCBM/LA/ALD SnO_2/PEDOT: PSS/PM6:L8-BO/PDINN/Ag, where the 1.77 eV-based WBG perovskite was used as front cell and the PM6:L8-BO (the chemical structures were displayed in Fig. S9.) based OSC was used as rare cell, as presented in Fig. 6(a). In Fig. 6(b), it shows the cross-section scan electron microscopy (SEM) image of POTSC, which declares that all the active and functional layers are deposited sequentially and completely. To get the photovoltaic characteristics, the *J-V* curves were tested, as shown in Fig. 6(c). It is noted that we can acquire a high photovoltaic performance with a V_{OC} of 2.15 V, a J_{SC} of 14.91 mA cm^{-2}, an FF of 73 %, and a PCE of 23.51 %, and the corresponding photovoltaic properties of front and rare cells are summarized in Table S4. To evaluate the reproducibility of POTSCs, the statistics on PCE distribution is provided in Fig. 6(d), where an average efficiency of 22.64 % is achieved. This means that the LA could realize high reproducibility in fabricating POTSCs. Furthermore, the SPO of POTSC was also examined at MPP tracking under continuous one sun illumination, as depicted in Fig. 6(e). It shows a stabilized efficiency of 23 % under a steady voltage of 1.77 V, confirming the excellent reliability in POTSC. In Fig. 6(f), it provided the EQE spectra of the corresponding WBG PSC and low-bandgap OSC in a 2 T tandem cell, respectively. It shows that this POTSC possesses a broad responsibility from 300 to 900 nm, and most of EQE values exceed 80 %, exhibiting excellent photocurrent matching. The integrated J_{SC} values from EQE curves for WBG PSC and OSC are 14.88 and 14.70 mA cm^{-2}, which agree well with the J_{SC} obtained from the corresponding *J-V* curves. To evaluate the function of LA as efficient ICL in POTSCs, we compared the results of V_{OC}-PCE statistics published in literature for the inverted perovskite-binary organic TSCs, as presented in Fig. 6(g) and Table S5. To the best of our knowledge, a V_{OC} of 2.15 V with a PCE of >23.5 % is one of the highest values in inverted organic-inorganic perovskite-binary organic TSCs. Interestingly, the introduction of LA in ICL also results in high device shelf lifetime, as shown in Fig. 6(h). Hence, these results demonstrate that the natural pigment LA could work as an efficient and stable interlayer in ICL for high-performance POTSCs.

3. Conclusion

To conclude, a natural pigment (LA) is utilized as an efficient CIL for WBG PSCs and TOPSCs. Owning to the introduction of LA CIL, the *WF* of Ag cathode is reduced distinctly, leading to matchable interfacial ohmic contact and thereby facilitating electron transport. Furthermore, LA CIL can slow down interfacial recombination and energy loss, resulting in the synergistic improvement on V_{OC}s and FFs in PSCs. Interestingly, LA demonstrates broad applicability as CIL in both WBG PSCs and TOPSCs, where WBG PSC gives a PCE of 18.48 % with a high V_{OC} of 1.32 V and a high FF of 81 %, and TOPSC exhibits a high PCE of 23.51 % with a V_{OC} of 2.15 V. These high V_{OC}s, FFs and PCEs are among the highest values both in 1.77 eV-based WBG PSC and TOPSC. In addition, the introduction of LA CIL also enhances the device stabilities in WBG PSC and TOPSC. Hence, reflecting from this study, the low-cost and environmentally friendly natural pigments would be a potential candidate to work as efficient CILs for constructing high-performance and stable PSCs and TOPSCs in future.

3.1. Experimental section

The details of materials, characterization, device fabrication and tests, and photophysical measurement are presented in the supporting information.

CRediT authorship contribution statement

Bin Zhang: Writing – review & editing, Writing – original draft, Supervision, Investigation, Formal analysis, Data curation, Conceptualization. **Yunqiang Du:** Investigation, Formal analysis, Data curation, Methodology. **Xinling Li:** Methodology. **Aiqin Li:** Methodology, Formal analysis. **Menglan Lv:** Writing – review & editing, Project administration, Supervision, Formal analysis. **Weile Guo:** Methodology. **Fei Guo:** Data curation, Resources, Methodology, Formal analysis. **Ergang Wang:** Writing – review & editing, Supervision, Project administration, Formal analysis.

Declaration of competing interest

The authors declare that they have no known competing financial interests or personal relationships that could have appeared to influence the work reported in this paper.

Acknowledgements

This work was supported by the National Natural Science Foundation of China (52373175), the Guizhou Provincial Basic Research Program (General Program) (No. MS[2025]603), the High-level Innovative Talents Foundation of Guizhou Province (QKHPTRC-GCC[2023]024), Natural Science Foundation of Guizhou Province (QKHPTRC-CXTD [2023]005), Science and Technology Innovation Team of Higher Education Department of Guizhou Province (QJJ[2023]053), Natural Science Foundation of Guizhou University (GZUTGH[2023]12) and Science and Technology Innovation Team of Guizhou University (GZUKCT[2023]01). E.W. further thanks the Swedish Research Council (2020-05223), the Swedish Research Council Formas (2023-01008), the Swedish Energy Agency (P2021-90067), and the Wallenberg Foundation (2022.0192) for financial support.

Appendix A. Supplementary data

Supplementary data to this article can be found online at https://doi.org/10.1016/j.cej.2025.167241.

Data availability

Data will be made available on request.

References

[1] A. Kojima, K. Teshima, Y. Shirai, T. Miyasaka, Organometal halide perovskites as visible-light sensitizers for photovoltaic cells, J. Am. Chem. Soc. 131 (17) (2009) 6050–6051, https://doi.org/10.1021/ja809598r.
[2] M. Liu, M.B. Johnston, H.J. Snaith, Efficient planar heterojunction perovskite solar cells by vapour deposition, Nature 501 (2013) 395–398, https://doi.org/10.1038/nature12509.
[3] H. Chen, C. Liu, J. Xu, A. Maxwell, W. Zhou, Y. Yang, Q. Zhou, A.S.R. Bati, H. Wan, Z. Wang, L. Zeng, J. Wang, P. Serles, Y. Liu, S. Teale, Y. Liu, M.I. Saidaminov, M. Li, N. Rolston, S. Hoogland, T. Filleter, M.G. Kanatzidis, B. Chen, Z. Ning, E. H. Sargent, Improved charge extraction in inverted perovskite solar cells with dual-site-binding ligands, Science 384 (2024) 189–193, https://doi.org/10.1126/science.adm9474.
[4] K. Zhao, Q. Liu, L. Yao, C. Değer, J. Shen, X. Zhang, P. Shi, Y. Tian, Y. Luo, J. Xu, J. Zhou, D. Jin, S. Wang, W. Fan, S. Zhang, S. Chu, X. Wang, L. Tian, R. Liu, L. Zhang, I. Yavuz, H. Wang, D. Yang, R. Wang, J. Xue, Peri-fused polyaromatic molecular contacts for perovskite solar cells, Nature 632 (2024) 301–306, https://doi.org/10.1038/s41586-024-07712-6.
[5] S. Liu, J. Li, W. Xiao, R. Chen, Z. Sun, Y. Zhang, X. Lei, S. Hu, M. Kober-Czerny, J. Wang, F. Ren, Q. Zhou, H. Raza, Y. Gao, Y. Ji, S. Li, H. Li, L. Qiu, W. Huang, Y. Zhao, B. Xu, Z. Liu1, H.J. Snaith, N.-G. Park, W. Chen, Buried interface molecular hybrid for inverted perovskite solar cells, Nature 632 (2024) 536–542, https://doi.org/10.1038/s41586-024-07723-3.

[6] P. Chen, Y. Xiao, S. Li, X. Jia, D. Luo, W. Zhang, H.J. Snaith, Q. Gong, R. Zhu, The promise and challenges of inverted perovskite solar cells, Chem. Rev. 124 (19) (2024) 10623–10700, https://doi.org/10.1021/acs.chemrev.4c00073.
[7] Qi Jiang, Kai Zhu, Rapid advances enabling high-performance inverted perovskite solar cells, Nat. Rev. Mater. 9 (2024) 399–419, https://doi.org/10.1038/s41578-024-00678-x.
[8] C. Li, Y. Chen, Z. Zhang, C. Liu, F. Guo, W. Ahmad, P. Gao, Pros and cons of hole-selective self-assembled monolayers in inverted PSCs and TSCs: extensive case studies and data analysis, Energy Environ. Sci. 17 (2024) 6157–6203, https://doi.org/10.1039/D4EE02492C.
[9] J. Lim, N.-G. Park, S.I. Seok, M. Saliba, All-perovskite tandem solar cells: from fundamentals to technological progress, Energy Environ. Sci. 17 (2024) 4390–4425, https://doi.org/10.1039/D3EE03638C.
[10] R. Lin, Y. Wang, Q. Lu, B. Tang, J. Li, H. Gao, Y. Gao, H. Li, C. Ding, J. Wen, P. Wu, C. Liu, S. Zhao, K. Xiao, Z. Liu, C. Ma, Y. Deng, L. Li, F. Fan, H. Tan, All-perovskite tandem solar cells with 3D/3D bilayer perovskite heterojunction, Nature 620 (2023) 994–1000, https://doi.org/10.1038/s41586-023-06278-z.
[11] M. Han, R. Zhou, G. Chen, Q. Li, P. Li, C. Sun, Y. Zhang, Y. Song, Unveiling the potential of two-terminal perovskite/organic tandem solar cells: mechanisms, status, and challenges, Adv. Mater. 36 (26) (2024) 2402143, https://doi.org/10.1002/adma.202402143.
[12] X. Guo, Z. Jia, S. Liu, R. Guo, F. Jiang, Y. Shi, Z. Dong, R. Luo, Y.-D. Wang, Z. Shi, J. Li, J. Chen, L.K. Lee, P. Müller-Buschbaum, D.S. Ginger, D.J. Paterson, Y. Hou, Stabilizing efficient wide-bandgap perovskite in perovskite-organic tandem solar cells, Joule 8 (9) (2024) 2542–2569, https://doi.org/10.1016/j.joule.2024.06.009.
[13] Z. Ying, X. Yang, X. Wang, J. Ye, Towards the 10-year milestone of monolithic perovskite/silicon tandem solar cells, Adv. Mater. 36 (37) (2024) 2311501, https://doi.org/10.1002/adma.202311501.
[14] E. Aydin, T.G. Allen, M.D. Bastiani, A. Razzaq, L. Xu, E. Ugur, J. Liu, S.D. Wolf, Pathways toward commercial perovskite/silicon tandem photovoltaics, Science 383 (6679) (2024) 162, https://doi.org/10.1126/science.adh3849.
[15] J. Liu, Y. He, L. Ding, H. Zhang, Q. Li, L. Jia, J. Yu, T.W. Lau, M. Li, Y. Qin, X. Gu, F. Zhang, Q. Li, Y. Yang, S. Zhao, X. Wu, J. Liu, T. Liu, Y. Gao, Y. Wang, X. Dong, H. Chen, P. Li, T. Zhou, M. Yang, X. Ru, F. Peng, S. Yin, M. Qu, D. Zhao, Z. Zhao, M. Li, P. Guo, H. Yan, C. Xiao, P. Xiao, J. Yin, X. Zhang, Z. Li, B. He, X. Xu, Perovskite/silicon tandem solar cells with bilayer interface passivation, Nature 635 (2024) 596–603, https://doi.org/10.1038/s41586-024-07997-7.
[16] Z. Qiang, Y. Wu, X. Gao, Y. Gong, Y. Liu, X. Zhao, H. Tian, W. Wang, C. Wang, W. Liu, J. Zong, J. Jiang, A scalable method for fabricating monolithic perovskite/silicon tandem solar cells based on low-cost industrial silicon bottom cells, Chem. Eng. J. 495 (2024) 153422, https://doi.org/10.1016/j.cej.2024.153422.
[17] K.O. Brinkmann, P. Wang, F. Lang, W. Li, X. Guo, F. Zimmermann, S. Olthof, D. Neher, Y. Hou, M. Stolterfoht, T. Wang, A.B. Djurišić, T. Riedl, Perovskite-organic tandem solar cells, Nat. Rev. Mater. 9 (2024) 202–217, https://doi.org/10.1038/s41578-023-00642-1.
[18] J. Yi, G. Zhang, H. Yu, H. Yan, Advantages, challenges and molecular design of different material types used in organic solar cells, Nat. Rev. Mater. 9 (2024) 46–62, https://doi.org/10.1038/s41578-023-00618-1.
[19] P. Ding, D. Yang, S. Yang, Z. Ge, Stability of organic solar cells: toward commercial applications, Chem. Soc. Rev. 53 (2024) 2350–2387, https://doi.org/10.1039/D3CS00492A.
[20] M.F.M. Noh, N.A. Arzaee, M.N. Harif, M.A.M. Teridi, A.R.b.M. Yusoff, A.W. M. Zuhdi, Defect engineering at buried interface of perovskite solar cells, Small Methods (2024), https://doi.org/10.1002/smtd.202400385.
[21] J. Wang, L. Bi, Q. Fu, A.K.-Y. Jen, Methods for passivating defects of perovskite for inverted perovskite solar cells and modules, Adv. Energy Mater. 14 (35) (2024) 2401414, https://doi.org/10.1002/aenm.202401414.
[22] M. Ye, C. He, J. Iocozzia, X. Liu, X. Cui, X. Meng, M. Rager, X. Hong, X. Liu, Z. Lin, Recent advances in interfacial engineering of perovskite solar cells, J. Phys. D. Appl. Phys. 50 (37) (2017) 373002, https://doi.org/10.1088/1361-6463/aa7cb0.
[23] S. Bi, X. Leng, Y. Li, Z. Zheng, X. Zhang, Y. Zhang, H. Zhou, Interfacial modification in organic and perovskite solar cells, Adv. Mater. 31 (45) (2019) 1805708, https://doi.org/10.1002/adma.201805708.
[24] J. Lee, H. Tüysüz, In-depth comparative study of the cathode interfacial layer for a stable inverted perovskite solar cell, ChemSusChem 14 (11) (2021) 2393–2400, https://doi.org/10.1002/cssc.202100585.
[25] P. Cai, L. Ding, Z. Chen, D. Wang, H. Peng, C. Yuan, C. Hu, L. Sun, Y.N. Luponosov, F. Huang, Q. Xue, Tetrabutylammonium bromide functionalized Ti3C2Tx MXene as versatile cathode buffer layer for efficient and stable inverted perovskite solar cells, Adv. Funct. Mater. 33 (30) (2023) 2300113, https://doi.org/10.1002/adfm.202300113.
[26] A. Yakusheva, D. Saranin, D. Muratov, P. Gostishchev, H. Pazniak, A.D. Vito, T. S. Le, L. Luchnikov, A. Vasiliev, D. Podgorny, D. Kuznetsov, S. Didenko, A.D. Carlo, Photo stabilization of p-i-n perovskite solar cells with bathocuproine: MXene, Small 18 (37) (2022) 2201730, https://doi.org/10.1002/smll.202201730.
[27] T. Zheng, H. Zhou, B. Fan, Y. Zhao, B. Jin, L. Fan, R. Peng, Designing conductive fullerenes ionene polymers as efficient cathode interlayer to improve inverted perovskite solar cells efficiency and stability, Chem. Eng. J. 415 (2021) 128816, https://doi.org/10.1016/j.cej.2021.128816.
[28] J.O. Obila, D.H. Ryu, S. Oh, J.H. Kim, R.J. Musembi, S. Lee, B.J. Kang, N.J. Jeon, E. O. Ayieta, S.H. Im, C.E. Song, Tin-based perovskite solar cells containing a perylene diimide cathode interlayer with a copper top electrode, ACS Energy Lett. 9 (3) (2024) 1090–1096, https://doi.org/10.1021/acsenergylett.3c02795.
[29] T. Wu, P. Xu, D. Wang, X. Jiang, F. Guo, S. Gao, Z. Ge, Y. Zhang, One-step synthesis of low-cost perylenediimide-based cathode interfacial materials for efficient inverted perovskite solar cells, Chem. Eng. J. 454 (2023) 140451, https://doi.org/10.1016/j.cej.2022.140451.
[30] T. Wu, D. Wang, Y. Lu, Z. Zheng, F. Guo, T. Ye, S. Gao, Y. Zhang, Multifunctional perylenediimide-based cathode interfacial materials for high-performance inverted perovskite solar cells, ACS Appl. Energy Mater. 4 (12) (2021) 13657–13665, https://doi.org/10.1021/acsaem.1c02339.
[31] A. Sharma, S. Singh, X. Song, D.R. Villalva, J. Troughton, D. Corzo, L. Toppare, G. Gunbas, B.C. Schroeder, D. Baran, A nonionic alcohol soluble polymer cathode interlayer enables efficient organic and perovskite solar cells, Chem. Mater. 33 (22) (2021), https://doi.org/10.1021/acs.chemmater.1c01430, 8602-8166.
[32] A. Wijesekara, M. Walker, Y. Han, D. Walker, S. Huband, R.A. Hatton, Enhanced stability of tin halide perovskite photovoltaics using a bathocuproine—copper top electrode, Adv. Energy Mater. 11 (48) (2021) 2102766, https://doi.org/10.1002/aenm.202102766.
[33] P. Hang, J. Xie, C. Kan, B. Li, Y. Zhang, P. Gao, D. Yang, X. Yu, Stabilizing fullerene for burn-in-free and stable perovskite solar cells under ultraviolet preconditioning and light soaking, Adv. Mater. 33 (10) (2021) 2006910, https://doi.org/10.1002/adma.202006910.
[34] Y. Du, C. Chen, Y. Zhao, J. Wang, Z. Chen, M. Lv, F. Zhang, Q. Xue, F. Guo, Y. Mai, B. Zhang, Phenanthroline-based low-cost and efficient small-molecule cathode interfacial layer enables high-performance inverted perovskite solar cells via doctor-blade coating, ACS Appl. Mater. Interfaces 16 (39) (2024) 52727–52738, https://doi.org/10.1021/acsami.4c07014.
[35] R. Wang, J. Xue, K.-L. Wang, Z.-K. Wang, Y. Luo, D. Fenning, G. Xu, S. Nuryyeva, T. Huang, Y. Zhao, J.L. Yang, J. Zhu, M. Wang, S. Tan, I. Yavuz, K.N. Houk, Y. Yang, Constructive molecular configurations for surface-defect passivation of perovskite photovoltaics, Science 366 (6472) (2019) 1509–1513, https://doi.org/10.1126/science.aay9698.
[36] N. Jia, P. Guo, K. Zhang, C. Liu, R. Chen, Z. Liu, Q. Ye, H. Wang, Defect passivation by natural piperine molecule enabling for stable perovskite solar cells with efficiencies over 23%, ACS Sustain. Chem. Eng. 10 (49) (2022) 16359–16367, https://doi.org/10.1021/acssuschemeng.2c05527.
[37] B. Liu, Y. Wang, Y. Wu, Y. Zhang, J. Lyu, Z. Liu, S. Bian, X. Bai, L. Xu, D. Zhou, B. Dong, H. Song, Vitamin natural molecule enabled highly efficient and stable planar n-p homojunction perovskite solar cells with efficiency exceeding 24.2%, Adv. Energy Mater. 13 (2) (2023) 2203352 https://doi.org/10.1002/aenm.202203352.
[38] X. Pang, J. Huang, C. Lin, Y. Zhang, N. Cheng, W. Zi, Z.-Z. Sun, Z. Yu, Z. Zhao, Buried interface regulation by bio-functional molecules for efficient and stable planar perovskite solar cells, Chem. Eur. J. 29 (14) (2023) e202202744, https://doi.org/10.1002/chem.202202744.
[39] X. Liu, Q. Geng, Y. Gao, S. Zhang, H. Yu, Y. Li, Q. Zhang, H. Zhong, C. Yao, X. Chu, Dual interfacial modifications by a natural organic acid enable high-performance perovskite solar cells with lead shielding, ACS Appl. Mater. Interfaces 16 (51) (2024) 71008–71018, https://doi.org/10.1021/acsami.4c13074.
[40] J. Wang, J. Li, Y. Zhou, C. Yu, Y. Hua, Y. Yu, R. Li, X. Lin, R. Chen, H. Wu, H. Xia, H.-L. Wang, Tuning an electrode work function using organometallic complexes in inverted perovskite solar cells, J. Am. Chem. Soc. 143 (20) (2021) 7759–7768, https://doi.org/10.1021/jacs.1c02118.
[41] C. Feng, X. Wang, Z. He, Y. Cao, Formation mechanism of PFN dipole interlayer in organic solar cells, Sol. RRL 5 (4) (2021) 2000753, https://doi.org/10.1002/solr.202000753.
[42] B. Zhang, Y. Zhao, C. Xu, C. Feng, W. Li, X. Qin, M. Lv, X. Luo, X. Qin, A. Li, Z. He, E. Wang, Perylene diimide-based low-cost and thickness-tolerant electron transport layer enables polymer solar cells approaching 19% efficiency, Adv. Funct. Mater. 34 (34) (2024) 2400903, https://doi.org/10.1002/adfm.202400903.
[43] G. Wang, K. Zhang, Z. Wang, J. Wang, R. Xu, L. Li, X. Xu, Y. Li, S. Xiao, S. Zheng, X. Li, S. Yang, Boosting performance and stability of inverted perovskite solar cells by modulating the cathode interface with phenyl phosphine-inlaid semiconducting polymer, Nano Energy 89 (2021) 106374, https://doi.org/10.1016/j.nanoen.2021.106374.
[44] C. Yu, J. Yang, Z. Bing, Y. Hu, B. Li, J. Huang, F. Li, Resolving the puzzle of charge carrier lifetime in znO by revisiting the role of oxygen vacancy, J. Phys. Chem. Lett. 15 (1) (2024) 1–8, https://doi.org/10.1021/acs.jpclett.3c03195.
[45] B. Zhang, Z. Pan, W. Li, Y. Zhao, X. Qin, A. Li, M. Lv, X. Qin, W. Guo, Z. He, E. Wang, Natural dextran as an efficient interfacial passivator for ZnO-based electron-transport layers in inverted organic solar cells, Adv. Energy Mater. (15) (2025) 2404297, https://doi.org/10.1002/aenm.202404297.
[46] G. Chen, F. Zhang, M. Liu, J. Song, J. Lian, P. Zeng, H.-L. Yip, W. Yang, B. Zhang, Y. Cao, Fabrication of high-performance and low-hysteresis lead halide perovskite solar cells by utilizing a versatile alcohol-soluble bispyridinium salt as an efficient cathode modifier, J. Mater. Chem. A 5 (34) (2017) 17943–17953, https://doi.org/10.1039/C7TA04995A.
[47] T. Wu, D. Wang, X. Jiang, X. Ge, F. Guo, T. Ye, S. Gao, Y. Zhang, Molecular regulation of perylenediimide and fluorene-based cathode interfacial materials for efficient inverted perovskite solar cells, Adv. Mater. Interfaces 9 (28) (2022) 2200923, https://doi.org/10.1002/admi.202200923.
[48] J. Shi, M.W. Samad, F. Li, C. Guo, C. Liu, J. Guo, Y. Zhang, J. Zeng, D. Wang, W. Ma, B. Xu, J. Yuan, Dual-site molecular dipole enables tunable interfacial field toward efficient and stable perovskite solar cells, Adv. Mater. 36 (44) (2024) 2410464, https://doi.org/10.1002/adma.202410464.
[49] Y. Zhao, J. Wu, W. Li, X. Qin, M. Lv, Y. Hua, W. Zhu, Z. He, B. Zhang, Morphology control realizes fast charge dissociation and transport in high-performance all-polymer solar cells, ACS Appl. Energy Mater. 7 (9) (2024) 4180–4189, https://doi.org/10.1021/acsaem.4c00534.

[50] S. Zhang, T. Xu, P. Wu, J. Pan, W. Zhang, W. Song, Halogen substitution of perinone-based cathode interfacial materials for high-efficiency inverted perovskite solar cells, J. Mater. Chem. C 12 (13) (2024) 4676–4681, https://doi.org/10.1039/D4TC00266K.

[51] N. Yan, Y. Cao, Z. Dai, L. Jiang, Y. Yang, T. Li, L. Li, S. Liu, Z. Fang, J. Feng, Heterogeneous seed-assisted *FAPbI3* crystallization for efficient inverted perovskite solar cells, Energy Environ. Sci. 17 (14) (2024) 5070–5079, https://doi.org/10.1039/D4EE01044B.

[52] K.O. Brinkmann, T. Becker, F. Zimmermann, C. Kreusel, T. Gahlmann, M. Theisen, T. Haeger, S. Olthof, C. Tückmantel, M. Günster, T. Maschwitz, F. Göbelsmann, C. Koch, D. Hertel, P. Caprioglio, F. Peña-Camargo, L. Perdigón-Toro, A. Al-Ashouri, L. Merten, A. Hinderhofer, L. Gomell, S. Zhang, F. Schreiber, S. Albrecht, K. Meerholz, D. Neher, M. Stolterfoht, T. Riedl, Perovskite-organic tandem solar cells with indium oxide interconnect, Nature 604 (2022) 280–286, https://doi.org/10.1038/s41586-022-04455-0.

[53] S. Jiang, R. Wang, M. Li, R. Yu, F. Wang, Z. Tan, Synergistic electrical and light management enables efficient monolithic inorganic perovskite/organic tandem solar cells with over 24% efficiency, Energy Environ. Sci. 17 (2024) 219–226, https://doi.org/10.1039/D3EE02940A.

[54] H. Yang, W. Chen, Y. Yu, Y. Shen, H. Yang, X. Li, B. Zhang, H. Chen, Q. Cheng, Z. Zhang, W. Qin, J.-D. Chen, J.-X. Tang, Y. Li, Y. Li, Regulating charge carrier recombination in the interconnecting layer to boost the efficiency and stability of monolithic perovskite/organic tandem solar cells, Adv. Mater. 35 (6) (2023) 2208604, https://doi.org/10.1002/adma.202208604.